Relaxation of a simulated lipid bilayer vesicle compressed by an atomic force microscope

Ben M. Barlow, Martine Bertrand, and Béla Joós*
Ottawa-Carleton Institute for Physics, University of Ottawa Campus, Ottawa, Ontario, Canada K1N 6N5
(Received 5 May 2016; revised manuscript received 21 August 2016; published 15 November 2016)

Using coarse-grained molecular dynamics simulations, we study the relaxation of bilayer vesicles, uniaxially compressed by an atomic force microscope cantilever. The relaxation time exhibits a strong force dependence. Force-compression curves are very similar to recent experiments wherein giant unilamellar vesicles were compressed in a nearly identical manner.

DOI: 10.1103/PhysRevE.94.052408

I. INTRODUCTION

Cells (the building blocks of life) are very complicated mechanical objects—eukaryotic cells especially so. The plasma membrane, a lipid bilayer with many protein inclusions, separates the cell from the outside environment. As model physical systems, lipid bilayer vesicles (vesicles) have been an attractive starting point for theoretical work, simulations, and experiments. Vesicles play an important role in cell function, e.g., storing and transporting substances throughout the cell. Their mechanical and dynamic properties are therefore of significance, not only for those functions, but also for the cell membrane whose basic structure is a lipid bilayer with a cytoskeleton and many inclusions.

In this paper our focus is not on static properties, but on the dynamics of the stress relaxation. In particular we observe that the relaxation time depends on the magnitude of the applied stress, increasing sharply in the limit of low stress. Further, we show that this behavior can be derived from the Helfrich and Servuss model [1] for undulating elastic membranes. This derivation predicts a *finite* maximum relaxation time, proportional to the membrane's surface area.

To investigate the viscoelastic properties of vesicles, we ran computer simulations wherein a vesicle is squeezed between two plates (Fig. 1). This procedure is relevant to experiments [2–8] which use an atomic force microscope (AFM) to poke and squeeze and stretch living cells and vesicles. An analogous experimental setup was used by Schäfer *et al.* [3] to investigate *static* properties of giant liposomes. But cells and vesicles are not deformed only in the laboratory. Inside our own bodies, every time the heart beats, every time we breathe, every time we flex a muscle of any kind—at every moment in cells all over the body, mechanical deformation of the membrane, cytoskeleton, and cell contents is occurring.

In this paper, we show that the relaxation time of compressed vesicles increases sharply with decreasing force in the limit of small force (and low surface tension). In that limit the membrane exhibits significant undulations which are reduced by the squeezing of the vesicle. This entropic contribution to the relaxation time increases sharply as the force is decreased. Helfrich and Servuss [1] (HS) have studied how membrane area expands with tension, and within their model we derive an expression for the relaxation time's force dependence. The connection between our vesicle's relaxation time and the applied stress may help to explain the wide variability of relaxation (and recovery) times reported for cells. The maximum relaxation time scales as the membrane's surface area, so the force dependence should be strong for cells and large vesicles as well. Scaled force-compression data are very similar to that reported for giant unilamellar vesicles (GUVs) by Schäfer *et al.* [3].

II. MODEL

We use coarse-grained molecular dynamics simulations to reproduce the basic characteristics common to all real lipid bilayer membranes. The model (Fig. 1) consists of approximately 140 000 particles in a simulation box with periodic boundary conditions. Our vesicle is the same as was used in [9] with reduced volume $\sim$1 (maximal volume without a pressure difference across the membrane), its membrane composed of coarse-grained lipids having one hydrophilic "head" particle and two hydrophobic "tail" particles. While relatively simple, these lipids are more than adequate for the present study. Our membrane exhibits thermal undulations, in-plane fluidity, intermonolayer friction, area compressibility, and bending rigidity, the basic features of fluid lipid bilayers. The model yields reasonable values for the area compressibility K_A, and bending rigidity κ (see Fig. 8 and Sec. III G as well as [9]). Despite the lipids' short chains, the membrane was not permeated by solvent, and lipid flips from one leaflet to the other were rare. We also note that there are advantages in using short lipids. There is the obvious reduction in simulation time, but the use of short lipids mitigates the disadvantages of small system size. Specifically, *short lipids reduce the ratio of membrane thickness to vesicle diameter*. Said ratio decreases with vesicle size.

The vesicles are constructed to attain a state where the internal and external fluid pressures are equal. The pressure difference has two contributions, potential and kinetic. The latter driven by temperature is significant and ensures that undulations persist in the bilayer up to lysis tension. At 3000 lipids, the membrane area is $\sim 10^3$ times the area per lipid, large enough to achieve the macroscopic properties described by continuum models. Figure 1 omits the outer fluid particles surrounding our small unilamellar vesicle. The explicit solvent filling and surrounding the vesicle is a Lennard-Jones fluid, at an initial density of 0.8 particles/L^3. (L is the unit of length, introduced in Sec. II B.) The vesicle is sandwiched between a substrate and an AFM cantilever—both consisting of fluidlike particles, constrained to remain in an fcc lattice. On the scale of our

*Corresponding author: bjoos@uottawa.ca

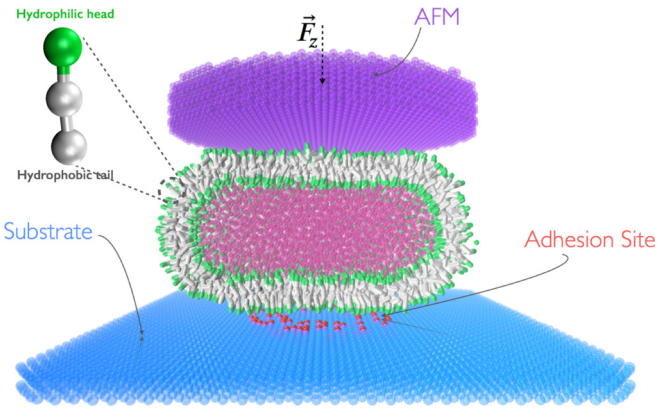

FIG. 1. Simulated vesicle undergoing parallel plate compression. In addition to the ordinary substrate particles, a bullseye of randomly distributed "sticky" particles was placed at the center of the substrate to ensure adhesion. Without this *adhesion site*, the vesicle would slip out from underneath the AFM cantilever. Coarse-grained lipid shown at upper left.

simulations, we treat a rounded AFM tip as approximately flat. For giant vesicles, this corresponds to a tipless AFM cantilever.

In molecular dynamics, pair potentials are defined which determine the force exerted by each particle on its neighbors and vice versa. To include thermal motion, there is an additional random force applied to each particle (generated by the simulation's "thermostat"). With the force on each particle determined by the thermostat and pair potentials, the time evolution of the system is governed by Newton's laws of motion. Our system is in the NVT ensemble, simulated using HOOMD-blue [10,11] with a DPD thermostat [12]. The DPD thermostat uses pairwise interactions to rescale particle velocities, which means that not only is temperature kept constant, but momentum is conserved—necessary for dynamic processes like the relaxation simulated here. The initial state was prepared using both the ESPResSo [13,14] and HOOMD-blue simulation packages. The Python packages matplotlib [15,16], MDAnalysis [17,18], and NumPy and SciPy [19,20] were used to plot and analyze our data.

A. Potentials

The two key interaction potentials in our simulation are the Lennard-Jones potential

$$V_{LJ} = 4E\left[\left(\frac{L}{r}\right)^{12} - s\left(\frac{L}{r}\right)^{6}\right], \tag{2.1}$$

and the soft-sphere potential

$$V_{SS} = ar^{-9}. \tag{2.2}$$

E is the unit of energy, introduced in Sec. II B. r is the particle separation. s is a parameter allowing the strength of the attractive portion of V_{LJ} to be tuned (default is $s = 1$). a tunes the strength of the soft-sphere (hydrophobic) potential.

V_{LJ} with $s = 1$ governs all nonbonded interactions between same-type particles, and between most particles of different types. The key exception is the hydrophobic tail-fluid interaction, which is governed by V_{SS}.

Bonds between monomers in the coarse-grained lipids are governed by a harmonic potential

$$V_{\text{harm}} = \frac{k}{2}(r - r_0)^2, \tag{2.3}$$

with $k = 5000E/L^2$. Bonds among particles making up the AFM probe as well as bonds between the substrate particles and their anchor points are implemented using V_{harm} with $k = 3000E/L^2$.

These are the same potentials as were used in [9,21], plus two additional potentials. First of the two is a cylindrical harmonic potential. This potential is used to keep the AFM centered and level during compression, by constraining its constituent particles to vertical motion. (The entire crystal is effectively *riding on rails*.) Second is V_{LJ} but with $s > 1$—the strength of the attractive term increased using the s parameter. This latter pair potential was used for the interaction of the "adhesion site" (in the center of the substrate in Fig. 1) with the lipid heads. The enhanced attraction causes the lipid heads to stick to the adhesion site, keeping the vesicle centered under the AFM.

B. Units

We denote our simulations' dimensionless units $L =$ length, $M =$ mass, $T =$ time, $E =$ energy, and $F =$ force. Figure axes are in dimensionless units when no S.I. units are specified. The conversion to dimensionful units (detailed in Appendix A) yields

$$\begin{aligned} L &\approx 0.6 \text{ nm} \\ M &\approx 8.5\times10^{-26} \text{ kg} \quad \approx \begin{pmatrix}\text{mass of three water molecules,}\\ \text{or four carbon atoms}\end{pmatrix} \\ T &\approx 3 \text{ ps} \\ E &\approx 4\times10^{-21} \text{ J} \quad \text{thermal energy per particle at room temperature } (T = 25\,^{\circ}\text{C}) \\ F &\approx 6.6 \text{ pN} \end{aligned} \tag{2.4}$$

These unit conversions are meant only as a rough guide to help scale the simulation in the context of lipid bilayer vesicles. If, instead of a vesicle, we were mapping our simulation to some other physical system, then different unit conversions would be invoked. (The validity of a given computer simulation might extend beyond the original system being studied.)

III. RESULTS

A. Relaxation time versus force

When we squeeze the vesicle, it relaxes to a new steady state with a characteristic time constant τ, which we call the relaxation time. We calculate this quantity by following the time evolution of the area expansion. A key result shown in Fig. 2 is that the *relaxation time depends strongly on the applied stress*, showing a sharp increase at low force.

We explain this result in Sec. III D using the HS model [1]. The sharp rise in the vesicle's relaxation time at low force arises from the effect of entropic undulations on the area expansion.

The time evolution of the area strain α after we activate the squeezing force is described as an exponential saturation

$$\alpha(t) = \alpha_\infty(1 - e^{-t/\tau}), \tag{3.1}$$

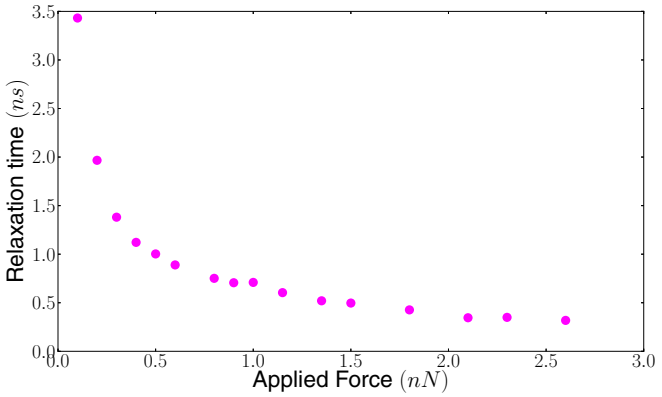

FIG. 2. Relaxation time plotted as a function of the squeezing force. The relaxation time shows a steep increase at low force. (Units are approximate; see Appendix A.)

as illustrated in Figs. 3 and 4. This type of viscoelastic creep response corresponds to the "Kelvin-Voigt" model, or the more general "Standard Linear Solid" (SLS) model. In this model the relaxation time is $\tau \sim \eta/K$, where η is a viscosity and K is an elastic modulus.

The *triangulated* area strain α^{tri} of the vesicle (Figs. 3 and 4) was used to obtain the relaxation times. This relative area change is calculated with a script used previously in [9,22], which implements Nina Amenta's "crust" algorithm [23] to triangulate the inner and outer leaflets of the vesicle (see Appendix B). In all further analysis, the apparent area of the vesicle (or "projected area") was used, as it is more amenable to modeling. There is therefore the assumption that the relaxation time does not depend on the specific way the area is calculated.

The full fitting function used in Figs. 3 and 4 is

$$\alpha^{\text{tri}}(t) = \begin{cases} \alpha_0^{\text{tri}} & \text{for } t < t_0 \\ \alpha_0^{\text{tri}} + \alpha_\infty^{\text{tri}}(1 - e^{-(t-t_0)/\tau}) & \text{for } t \geqslant t_0 \end{cases}. \quad (3.2)$$

Combining the creep response at $t \geqslant t_0$ with a flat line at $t < t_0$—the initial time t_0 being a free parameter—gives a more robust fit.

Even at relatively high forces ($>100F$), fluctuations in the vesicle's surface area are fairly large—on the same order of magnitude as the mean area expansion. For this reason, when

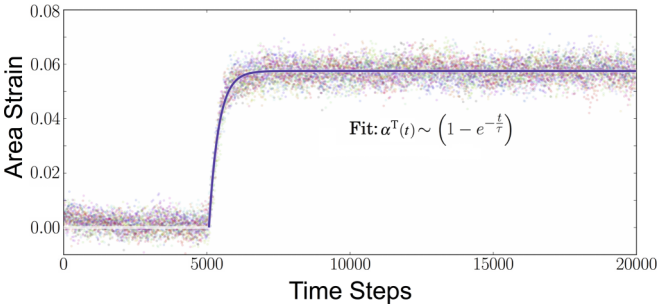

FIG. 3. Ensemble fit to creep response of the bilayer's triangulated area at $F_z = 100\text{F}$. For each value of the applied force, data from multiple simulations are fit as one time series. This helps to reduce the uncertainty on the relaxation time, by reducing the influence of noise from any particular simulation on the fit.

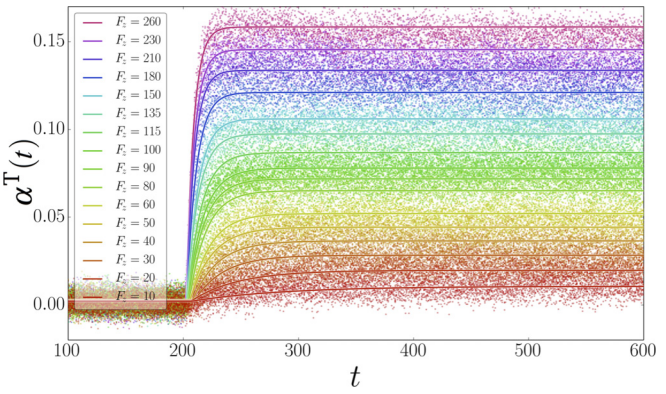

FIG. 4. Triangulated area expansion time series of vesicle at different forces (the force increases from bottom to top). Squeezing force is indicated by elevation, with bottom (red online) $= 10F$ and top (violet online) $= 260F$. Solid lines indicate fits to triangulated area $\alpha(t)$ from which relaxation times are obtained.

fitting for the relaxation time at a given force, data from multiple equivalent simulations are superposed and then fit as a single time series (see Fig. 3). That is, the relaxation time is fit to an ensemble of simulations. This way, the influence of random fluctuations from any particular time series is reduced.

B. Projected area expansion versus force

Due to thermal undulations, the surface area of a vesicle as measured in the laboratory will be less than the true surface area of its membrane. What one actually measures is the surface area of an *apparent surface*—the surface one gets by smoothing over the rapid fluctuations in membrane shape (see Appendix C). That is why the distinction is made between "apparent" or "projected" versus true surface area of the membrane.

Figure 5 shows our simulated vesicle's projected surface area versus force. Both leaflets are shown. The increase is logarithmic at low force and linear at high force.

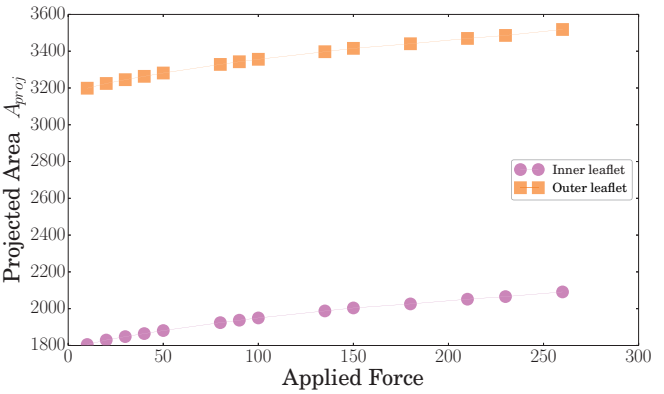

FIG. 5. Projected area (area of apparent surface; see Appendix C) of the bilayer vs force. Each leaflet is plotted separately.

C. Helfrich-Servuss (HS) model

To establish a physical basis for the force dependence of the relaxation time τ (Fig. 2), we begin by introducing the HS model [1], which is used in the next section to derive an expression for the relaxation time as a function of tension.

Membranes behave as entropic springs. Thermal agitation excites undulations in the vesicle membrane. If A is the zero temperature area of the membrane, the undulations will reduce the apparent (or projected) area by ΔA (negative at zero tension γ). When the membrane tension γ is increased, these undulations are reduced (ΔA approaches zero). This flattening of undulations by surface tension reduces the number of microstates (shapes) available to the vesicle, decreasing its entropy—just as pulling the ends of an entropic spring reduces the number of states available to it. If we increase the surface tension beyond the point at which undulations are largely suppressed, direct stretching of the membrane dominates. This true stretching is called "direct area expansion" whereas flattening undulations increases the apparent surface area of the membrane without actually stretching it. The *observed* area (also known as "apparent" or "projected" area) expansion results from a combination of these two effects.

In 1984 Helfrich and Servuss [1] derived an expression relating the relative change in a membrane's projected area ΔA to its surface tension γ:

$$\alpha(\gamma) \equiv \left(\frac{\Delta A}{A}\right)_{\gamma>0} = \underbrace{\frac{k_B T}{8\pi\kappa} \ln\left(\frac{\frac{\zeta}{A}+\frac{\gamma}{\kappa}}{\frac{\zeta}{a}+\frac{\gamma}{\kappa}}\right)}_{\text{entropic}} + \underbrace{\frac{\gamma}{K_A}}_{\text{direct}}, \tag{3.3}$$

where K_A, κ, A, and a are the membrane's area compressibility modulus, bending rigidity, unstressed area, and area per lipid, respectively. k_B is Boltzmann's constant, T is the temperature, and ζ is a parameter which depends on membrane shape (e.g., $\zeta = \pi^2$ for a planar membrane, and for a sphere $\zeta = 24\pi$). A mnemonic for Eq. (3.3) is

$$\alpha(\gamma) = \alpha_{\text{entropic}}(\gamma) + \alpha_{\text{direct}}(\gamma); \tag{3.4}$$

where $\alpha_{\text{entropic}}(\gamma)$, the first term in Eq. (3.3), is negative (tending to zero as $\gamma \to \infty$) since it measures the portion of membrane area A absorbed by undulations.

Vesicle size matters: larger membranes have more of their surface area hidden in undulations. In other words, $\alpha_{\text{entropic}}(\gamma)$ is more negative for larger A [see Eq. (3.3)]. Since wavelengths present in the bilayer are limited by the vesicle circumference, the spectrum of undulations is constrained by vesicle size. In fact, as $\gamma \to 0$ the undulations' mean square amplitude (which is dominated by the longest wavelengths present) scales as the membrane area [1].

Evans and Rawicz [24] studied the area expansion of vesicles subject to tensions $10^{-7} \leqslant \gamma \leqslant 10^{-3}$ N/m, and observed a logarithmic dependence at low tension followed by a linear dependence at larger tensions—consistent with the HS model. Further empirical support for the HS model was provided by Dimova *et al.* [25]. In this case, GUVs were deformed using electric fields, and their area expansion plotted against the resulting membrane tension.

More recent experiments (see Fig. 2 of Mell *et al.* [26]) have shown that the undulation spectrum $P = P_{\text{HS}}(\ell,\gamma)$ [Eq. (D4)] used in deriving the HS model [1] departs from experimental spectra at high wave number ℓ. In Appendix D we use the spectrum $P_{\text{Mell}}(\ell,\gamma)$ [Eq. (D5)] to derive a "revised HS model":

$$\alpha(\gamma) \approx \underbrace{\frac{k_B T}{8\pi\kappa} \ln\left(\frac{\frac{\zeta}{A}+\frac{\gamma}{\kappa}}{\frac{\zeta}{a}+\frac{\gamma}{\kappa}}\right) + \frac{3k_B T}{\pi h^2 K_A} \ln\left(\frac{1+\frac{h R\zeta}{2A}}{1+\frac{h R\zeta}{2a}}\right)}_{\text{entropic}} + \underbrace{\frac{\gamma}{K_A}}_{\text{direct}}. \tag{3.5}$$

The above correction alters α_{entropic} in Eq. (3.3), shifting it by a term which is independent of the surface tension. Being independent of the tension, this correction does not alter our model for the relaxation time, as we will see below.

D. Derivation of relaxation time

We now proceed to derive the relaxation time using the HS model as the starting point. From linear viscoelasticity theory, we have

$$\tau \sim \frac{\eta}{K}. \tag{3.6}$$

So the viscosity η and elastic modulus K need to be specified. The most physically appropriate viscosity is called the *dilatational-surface viscosity* [27,28] η_d—the viscosity associated with stretching the membrane, which we assume to be ≈const so that

$$\tau \propto \frac{1}{K}. \tag{3.7}$$

To obtain K we return to the heart of elasticity theory. Hooke's law suggests a more general definition for K: For small $\Delta(\cdot)$ we know that

$$\Delta(\text{strain}) = \frac{1}{K}\Delta(\text{stress}) \approx \left(\frac{\partial(\text{strain})}{\partial(\text{stress})}\right)\Delta(\text{stress}). \tag{3.8}$$

In the case of a stretching membrane strain $= \alpha$ (relative increase in the apparent area) and stress $= \gamma$ (the surface tension), so that

$$\frac{1}{K} \equiv \frac{\partial(\text{strain})}{\partial(\text{stress})} = \frac{\partial\alpha}{\partial\gamma} \tag{3.9}$$

defines the effective modulus K of the bilayer (in the vicinity of a specific value of γ).

With $\alpha(\gamma)$ specified by Eq. (3.5) [which turns out to be equivalent to Eq. (3.3) in our case, since the second entropic term does not depend on γ], Eq. (3.9) yields

$$\frac{1}{K} = \frac{1}{K_A} + \underbrace{\frac{k_B T}{8\pi\kappa}}_{\text{“}M\text{”}} \left\{\frac{1}{\frac{\zeta\kappa}{A}+\gamma} - \frac{1}{\frac{\zeta\kappa}{a}+\gamma}\right\}. \tag{3.10}$$

Note that Eq. (3.10) includes temperature, bending modulus, and area compressibility.

Returning to Eq. (3.6), which relates relaxation time, viscosity and elasticity, Eq. (3.10) predicts (via the HS model) a relaxation time

$$\tau(\gamma) \sim \frac{\eta}{K} \approx \eta\left(\frac{1}{K_A} + \frac{M}{\frac{\zeta\kappa}{A}+\gamma} + \frac{M}{\frac{\zeta\kappa}{a}+\gamma}\right). \tag{3.11}$$

Since $a \ll A$ and our simulations occur in the regime $\gamma \ll \frac{\zeta\kappa}{a}$, the term $\frac{1}{\frac{\zeta\kappa}{a}+\gamma} \approx \frac{a}{\zeta\kappa}$ and can be dropped from Eq. (3.10).

Equation (3.11) then simplifies to

$$\tau(\gamma) \sim \frac{\eta}{K} \approx \eta\left(\frac{1}{K_A} + \frac{M}{\frac{\zeta\kappa}{A} + \gamma}\right). \tag{3.12}$$

The relaxation time approaches a *finite* limit as the tension vanishes, and at high tension it decreases asymptotically toward (η/K_A) :

$$\tau(\gamma) \approx \eta\left(\frac{1}{K_A} + \frac{MA}{\zeta\kappa}\right) \quad \text{for vanishing tension, and}$$
$$\tau(\gamma) \approx \eta\left(\frac{1}{K_A} + \frac{M}{\gamma}\right) \quad \text{for larger tensions, i.e., } \gamma \gg \frac{\zeta\kappa}{A}. \tag{3.13}$$

The low-tension limit of τ increases as the surface area of the membrane, predicting longer relaxation times for larger vesicles and cells at low tension. The high-tension limit agrees with the observation by Dimova and co-workers [27,28] that for giant vesicles near lysis tension $\tau \sim \frac{\eta}{\gamma}$. Their result was justified through dimensional analysis.

A phenomenological form consistent with both the low and high tension limits [Eq. (3.13)] is

$$\tau \approx C_1 + \frac{C_2}{C_3 + \gamma}, \tag{3.14}$$

where C_1 is the high-tension asymptotic limit and $C_1 + \frac{C_2}{C_3}$ is the finite limit as $\gamma \to 0$. At low tension, the vesicle shape remains nearly spherical. At high tension, the vesicle shape is again approximately constant, this time resembling a wheel of cheese. So at both limits $\zeta \approx$ const, and Eq. (3.14) (derived from the HS model) is valid. Going a step further, in Sec. III F we fit the entire $\tau(\gamma)$ curve with this function, which succeeds as a phenomenological model and yields an estimate of (η/K_A).

E. Tension versus force

In the foregoing analysis we arrived at a model for the vesicle's relaxation time τ *as a function of the surface tension* γ [Eqs. (3.12)–(3.14) above]. The goal now is to apply that model to the simulated vesicle. However, our simulation data gave the relaxation time *as a function of the squeezing force* F_z (Fig. 2), not of the tension. (The tension in the membrane is not an explicit parameter of our MD simulations, but rather is an *effect* of the squeezing force F_z.) We therefore *need to know how* γ *varies as a function of* F_z.

The surface tension $\gamma(F_z)$ was calculated from the differential work dW done in deforming the vesicle. At each value of the squeezing force the vesicle was allowed to equilibrate, then the projected area, pressure, and volume were measured (e.g., Fig. 5). To approximate the surface tension at equilibrium as a function of the force, these measurements were used to obtain the tension from a relationship between equilibrium quantities, so the approximation of quasistatic deformation is applicable [Eqs. (3.15) and (3.16)]. Since forms of deformation other than area expansion also contribute to dW, the contribution due to γ had to be extracted from the total work.

Because our system is NVT, the differential mechanical work dW done by the AFM (while squeezing the vesicle) is equal to the change in the system's free energy $d\mathcal{F}$:

$$T = \text{const} \Rightarrow d\mathcal{F} = dW. \tag{3.15}$$

This is useful, since the surface tension γ can be defined in terms of the differential free energy,

$$d\mathcal{F} = \gamma dA - \sum_j P_j dV_j, \tag{3.16}$$

of the system (i.e., vesicle and solvent). The sum over j reads

$$\sum_j ()_j = ()_{\text{inner fluid}} + ()_{\text{membrane}} + ()_{\text{outer fluid}}. \tag{3.17}$$

The γdA term is the work done increasing the area of the membrane, and the sum over $P_j dV_j$ accounts for other work which may be done compressing or expanding the volume of the inner or outer fluid and of the membrane. Combining Eqs. (3.15) and (3.16) and dividing by dA gives

$$\gamma = \frac{dW}{dA} + \sum_j P_j \frac{dV_j}{dA}. \tag{3.18}$$

Everything on the right hand side of Eq. (3.18) is a function of F_z—the squeezing force. The $P_j(F_z)$, the $dV_j(F_z)$, $dA(F_z)$, and $dz(F_z)$ are obtained by curve-fitting (then numerically differentiating) the pressures, volumes, area, and AFM cantilever height (respectively) as functions of F_z. (Various regions' volumes and the membrane area are obtained by curve-fitting the vesicle's inner and outer surfaces as explained in Appendix C.) Knowing $dz(F_z)$ and $dA(F_z)$ also takes care of

$$\frac{dW}{dA} = F_z\left(\frac{dz}{dA}\right), \tag{3.19}$$

completing Eq. (3.18).

F. Relaxation time versus tension

We are now able to plot $\tau(\gamma)$—the relaxation time as a function of surface tension. In Fig. 6 we plot and fit $\tau(\gamma)$ using Eq. (3.14). Though the fit extends beyond small $\Delta\gamma$, it does estimate η/K_A from the asymptote at high tension, which is unchanged in more complicated fitting functions.

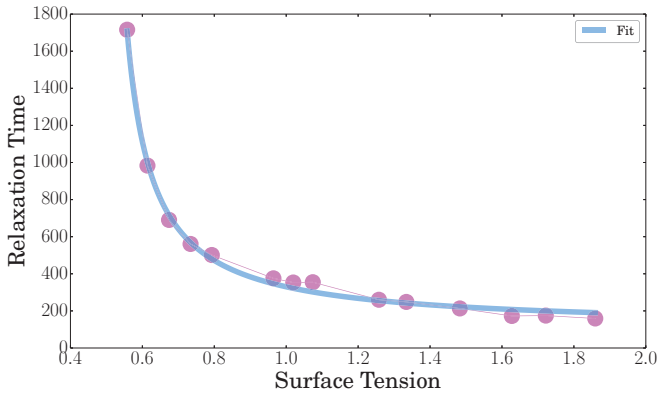

FIG. 6. Relaxation time vs surface tension, fit to Eq. (3.14). Derived out of the HS model, $\tau(\gamma)$ [Eq. (3.12)] leads to a correct description of the force dependence of the relaxation time.

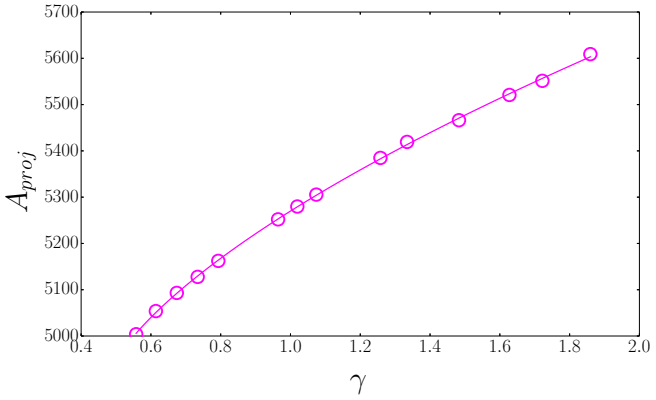

FIG. 7. Projected area vs surface tension. The tension (x axis) has been estimated via the work done compressing the vesicle [see Eq. (3.18)].

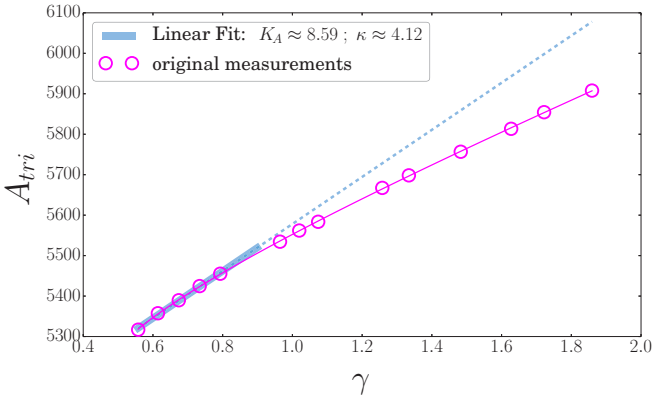

FIG. 8. Triangulated area vs surface tension. The tension (x axis) has been estimated via the work done compressing the vesicle [see Eq. (3.18)]. K_A is estimated using a linear fit to the low tension regime (see [31]). The bending rigidity is $\kappa = K_A l^2/48$, where l is the bilayer thickness [32]. The K_A returned by this fit agrees with that obtained by Bertrand and Joós [9] (flat bilayer, identical lipids) to within 3%.

This fit (blue line) gives $\frac{\eta}{K_A} \approx 108 \pm 16T$, which corresponds to a viscosity

$$\eta \approx 900FT/L \approx 3.1 \times 10^{-11}\ \text{Ns/m}. \tag{3.20}$$

Interestingly, this viscosity is $\approx 3\times$ the value of η_s (*shear*-surface viscosity) reported by den Otter *et al.* [29] for simulated DPPC bilayers. (*Dilatational*-surface viscosity η_d and *shear*-surface viscosity η_s have equivalent dimensions.) One might expect our η to be smaller than that of [29] since they used longer, two-tailed lipids. However for real lipid bilayers, the *dilatational*-surface viscosity η_d can be two orders of magnitude [27,28] larger than η_s. Given this fact, it is actually quite reasonable that our η should be larger than [29]'s η_s as well.

G. Area expansion versus tension

Figure 7 shows the projected area versus tension. The nonlinear regime at low tension is characteristic of the entropic behavior predicted by the HS model.

In Fig. 8 we estimate $K_A \approx 8.6\frac{E}{L^2}$ using a linear fit to the triangulated surface area, in the low-tension regime. This value compares well with previous simulations using similar lipids under similar conditions (~8.8 [9], ~11.0 [30], ~13.0 [31], ~12.0–13.6 [21,32]). Since K_A increases with tail length [33], it is reasonable to expect that our value will be at the low end of the spectrum. Converting our K_A into dimensionful units gives $K_A \approx 0.1$ N/m, which is reasonable when compared with experimental values—e.g., AFM indentation of supported bilayers $K_A \sim 0.12$ N/m [34], and micropipette aspiration of giant vesicles $K_A \sim 0.18$ N/m [35], ~ 0.13–0.64 N/m [24]. A quadratic fit to the triangulated area, like that found in Eq. (18) of [31], gives the same K_A, but requires an additional free parameter.

H. Vertical compression Δz

In Fig. 9 the vertical compression is scaled as a fraction of the maximum compression which the (respective) vesicle can withstand. The scaled GUV data (modified from Schäfer *et al.* [3]) and our simulation data are very similar, in spite of (i) the immense difference in size and (ii) the fact that our simulations use a *compressible* fluid—experimental buffer solutions are generally incompressible. This suggests that it is the physical character of the undulating *membrane*—rather than the solvent—that determines the force-compression curve of a fluid-filled vesicle. This result is supported by the analysis of Moreno-Flores and Benítez [36], who found that a vesicle's force-compression curve depends on the properties of its membrane and not on its size.

Our compression data begins at $F_z = 10.0F$, whereas the data from Schäfer *et al.* [3] begins much closer to $F_z = 0$. For this reason, we make the comparison using $\Delta F_z = (F_z - F_{z_0})$ on the x axis, and $\Delta z = (z - z_0)$ on the y axis [with $z_0 = z(F_{z_0})$].

We see from Fig. 9 that Δz and ΔA (Fig. 5) have the same form, however the logarithmic regime in Δz is exaggerated compared with that of ΔA. This is because initially $\Delta z(F_z)$ increases more rapidly than $A(F_z)$.

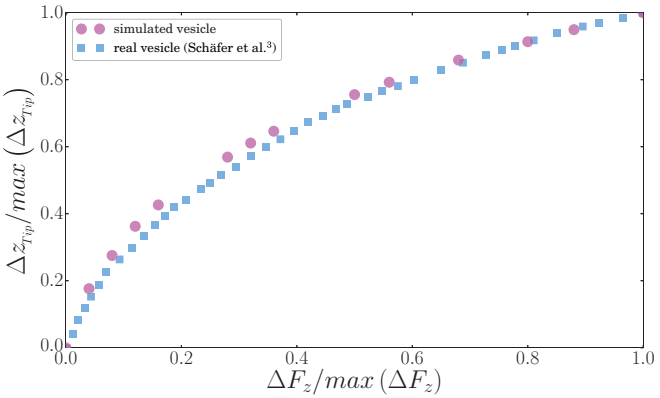

FIG. 9. Vertical compression: Relative height change as a function of applied force. The similarity between simulation and experimental data (modified from [3]) is striking.

IV. DISCUSSION

The relaxation time τ increases strongly at low tension; essentially $\tau(\gamma) \sim (\gamma + \text{const})^{-1}$ in this regime. This result follows from the Helfrich and Servuss model [1] (HS model), which describes the steady-state area expansion of bilayer membranes as a function of surface tension. The form of $\tau(\gamma)$ given in Eq. (3.11) (derived using the HS model) predicts that a vesicle's relaxation time will *depend on its size only at low tension* [see Eq. (3.13)]. Likewise at high tension the relaxation time is predicted to be *independent of the vesicle size*.

At low tension, flattening of undulations is the dominant form of relaxation (apparent area expansion). Vesicle size affects relaxation time by limiting the maximum wavelength and amplitude of these vibrational modes. At high tension, direct stretching of the membrane dominates, so the size effect on the undulations does not show up in τ.

The HS model describes membrane *area expansion* $\alpha(\gamma)$ as the combined effect of flattening entropic undulations and direct stretching. The model predicts that our measured area expansion should exhibit curvature in the low tension regime and linearity at high tension, which is what is seen in Fig. 7.

Further analysis in terms of the HS model allowed us to estimate the membrane viscosity, via a curve fit to $\tau(\gamma)$. The estimated surface viscosity [Eq. (3.20)] compares well with that observed for similar bilayers [29].

V. CONCLUSIONS

We report a strong dependence of the relaxation time on applied force (Fig. 2). The effect is greatest at low tension, due to flattening of undulations, but persists until lysis. Since undulations have been observed in real vesicles and cells [37], the force dependence should be present in them as well. Using the Helfrich and Servuss model [1] we predict that the effect (in the low force regime) should scale as the surface area (i.e., radius^2) of the membrane. Hence the dependence should be strong in real cells and giant vesicles, since their membranes are orders of magnitude larger than our small simulated vesicle.

Relaxation times vary widely in the literature [2,38–41], and some of this variation may be explained by the results presented above. Cells adhere very strongly to some surfaces, and weakly to others depending, e.g., on the stiffness of the substrate [42,43]. Strong adhesion suppresses undulations, thereby weakening the force dependence of τ. Experiments are also carried out under different tip conditions [44]. We therefore expect the relaxation time to depend strongly on the applied force and on the preexisting tension in the membrane—in short, on the experimental setup.

ACKNOWLEDGMENT

The authors acknowledge support from the Natural Sciences and Engineering Research Council (Canada).

APPENDIX A: CONVERSION TO DIMENSIONFUL UNITS

As stated, these unit conversions are presented only as a guideline—an approximate scaling of our model to lipid bilayer vesicles. The validity of the model is not restricted to vesicles. Should this simulation prove relevant to another physical system, another set of unit conversions could of course be invoked.

The procedure summarized here is based on that used by Goetz and Lipowski [21]. The energy unit (Lennard-Jones energy) in these simulations is defined $E = k_B T$. The Lennard-Jones fluid is meant to represent water at standard ambient temperature and pressure, so $E \approx 4 \times 10^{-21}$ J.

M is the particle mass. That is, every simulated particle is assigned the same mass: $m_j \equiv M$. A lower-bound on M is the mass of a single H_2O molecule ($\approx 3 \times 10^{-26}$ kg). Beads making up the tails of the simulated lipids provide an upper bound as they may represent up to six CH_2 molecules, so that $M \lesssim 14 \times 10^{-26}$ kg.

A lower bound for L (the Lennard-Jones length) is the average separation between two solvent molecules. For water, this is $\approx$0.31 nm. If a lipid tail bead represents at most six CH_2 groups, then the maximum distance between these beads along the lipid chain is six carbon-carbon bond lengths ($\approx$0.9 nm).

The unit of simulation time is $T = \sqrt{ML^2/E}$, and the force unit is $F = E/L$. Plugging in the above conversions yields $T \approx 2.8$ ps, and $F \approx 6.6$ pN.

APPENDIX B: SURFACE AREA OF BILAYER—TRIANGULATED SURFACE

The relaxation process was observed via the triangulated surface area, which is a direct measurement of the surface area of the vesicle. Triangulation: the bilayer's inner and outer leaflets are each approximated as tessellated surfaces, composed of triangles whose vertices are located at the lipid heads. Adding up the surface area of all the triangles composing the tessellated surface gives its total surface area—which we call the "triangulated area" of the membrane. The triangulated area is much closer to the true area of the membrane, rather than its apparent (i.e., "projected") area.

The derivation of $\tau(\gamma)$ in Sec. III D was done in terms of projected area, but relaxation times were obtained by fitting the *triangulated* (rather than projected) area. This complication does not harm the analysis. Notice that the direct area expansion term in Eq. (3.3) is $\frac{\gamma}{K_A}$, so direct stretching of the membrane is nonzero even at low tension (when flattening of undulations dominates the relaxation). Equation (3.3) [1] treats undulation flattening (α_{entropic}) and direct stretching (α_{direct}) like two springs in series[1] which relax simultaneously—pulling on either spring stretches both.

In short, we assume that there is one relaxation time, the time required for the system to reach steady state. Using a wave expansion of the undulations, Helfrich and Servuss calculated the apparent area of a membrane. So this is what was used in our theory. In numerical simulations triangulation methods can accurately estimate the surface area of the membrane. The relaxations times were obtained from the time variation of the triangulated area.

[1]Squeezing the vesicle increases its internal pressure, which increases membrane tension—"pulling on the springs."

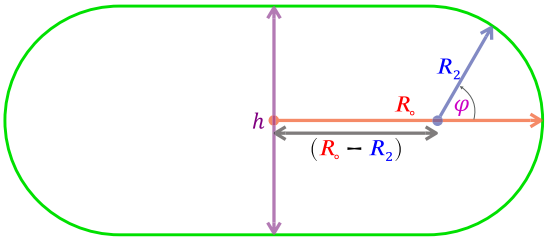

FIG. 10. Parametrization of a compressed vesicle (cf. Fig. 11). In the context of projected area and membrane undulations, this profile delineates the apparent surface of the vesicle. The shape of the compressed vesicle is well approximated by a "filled torus"—a doughnut without a hole. This approximation of the true surface is the same as was used by [3,45] and detailed in [46]. The variable names have been chosen to match those of [3] for ease of comparison. Coordinates: In this figure, h lies along the z axis. ϕ lies in the xy plane. $\varphi = \arctan(z/R_2)$.

APPENDIX C: SURFACE AREA OF BILAYER—APPARENT SURFACE

The apparent area expansion of vesicles is described by the HS model [1] [see Eq. (3.3)]. To measure the apparent area, the vesicle shape is parametrized (Fig. 10) and curve-fit (Fig. 11).

The free surface of the compressed vesicle (curved region in Figs. 10 and 11) is described by the position vector

$$\mathbf{r}(\phi,z) = \rho(z)\hat{\mathbf{e}}_\rho(\phi) + z\hat{\mathbf{e}}_z \qquad \begin{matrix} 0 \leqslant \phi < 2\pi \\ -\frac{h}{2} \leqslant z \leqslant \frac{h}{2} \end{matrix} \tag{C1}$$

in cylindrical coordinates (ρ,ϕ,z) with

$$\rho(z) = (R_0 - R_2) + \sqrt{R_2^2 - z^2}, \tag{C2}$$

and

$$\hat{\mathbf{e}}_\rho(\phi) = \cos\phi\hat{\mathbf{e}}_x + \sin\phi\hat{\mathbf{e}}_y. \tag{C3}$$

Curve-fitting the free surface allows us to parametrize the vesicle's *entire* apparent surface—from which we calculate the apparent area.

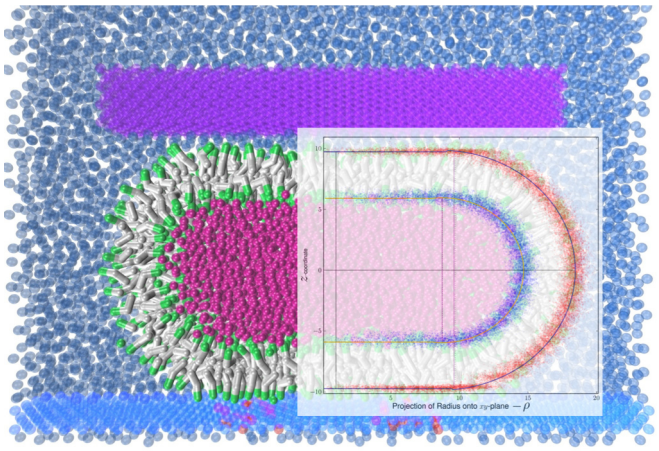

FIG. 11. Vesicle profile and the corresponding fit which measures the parameters h, R_0, and R_2 shown in Fig. 10.

APPENDIX D: REVISED HELFRICH-SERVUSS MODEL

As demonstrated in Fig. 2 of Mell *et al.* [26], the undulation spectrum $P = P_{\mathrm{HS}}(\ell,\gamma)$ that was used by Helfrich and Servuss [1] to derive the HS model departs from experimental fluctuation spectra at high wave number ℓ.

The relevance of this to the model that we presented for the vesicle's relaxation time $\tau(\gamma)$ is as follows: We model the compressed vesicle's relaxation time as a function of tension γ, in terms of an effective stiffness $K(\gamma)$ and viscosity η:

$$\tau \sim \frac{\eta}{K} \sim K^{-1}(\gamma), \tag{D1}$$

with $K^{-1} = \frac{\partial\alpha}{\partial\gamma}$. α, which denotes the relative change in a membrane's apparent area due to the competing effects of entropic undulations and surface tension, is modelled using the expression derived by Helfrich and Servuss [1]. The HS model contains two terms

$$\alpha(\gamma) = \alpha_{\mathrm{entropic}}(\gamma) + \alpha_{\mathrm{direct}}(\gamma). \tag{D2}$$

The first term gives the fraction of membrane area "absorbed" by undulations, reducing the "apparent area" of the membrane, and the second term accounts for direct stretching of the membrane by surface tension.

Here we are concerned only with the former, "entropic" term. To obtain it, Helfrich and Servuss integrate over the spectrum of undulations

$$\alpha_{\mathrm{entropic}}(\gamma) \propto \int_{\ell_{\min}}^{\ell_{\max}} \ell^3 P_{\mathrm{HS}}(\ell,\gamma)d\ell, \tag{D3}$$

where Eq. (9b) of Helfrich and Servuss (1984) gives the spectrum as

$$P_{\mathrm{HS}}(\ell,\gamma) \approx \frac{k_B T}{\gamma\ell^2 + \kappa\ell^4}. \tag{D4}$$

Since in our model $\tau(\gamma) \sim \frac{\partial\alpha}{\partial\gamma} = \frac{\partial}{\partial\gamma}(\alpha_{\mathrm{entropic}} + \alpha_{\mathrm{direct}})$, the undulation spectrum $P(\ell,\gamma)$ directly affects our model of $\tau(\gamma)$ through $\alpha_{\mathrm{entropic}}$.

Having arrived at the relevant point, we ask: Do the experimental spectra $P_{\mathrm{Mell}}(\ell,\gamma)$ in [26] differ from the approximation used by Helfrich and Servuss in such a way as to alter our model of $\tau(\gamma)$? We claim that the answer is "no": Eq. (16a) in [26] gives the bimodal spectrum

$$P_{\mathrm{Mell}}(\ell,\gamma) \approx \frac{k_B T}{\gamma\ell^2 + \kappa\ell^4} + \left(\frac{12R}{hK_A}\right)\frac{k_B T}{\ell^2 + \frac{1}{2}hR\ell^4}, \tag{D5}$$

which was fit to their observations. The departure of the observed spectra from the HS model can be expressed by writing

$$P_{\mathrm{Mell}}(\ell,\gamma) = P_{\mathrm{HS}}(\ell,\gamma) + f(\ell). \tag{D6}$$

That is to say, the experimental spectra differ from the HS model by a term which *does not depend on* γ. Hence while the spectrum $P_{\mathrm{Mell}}(\ell,\gamma)$ adds another entropic term $\alpha'_{\mathrm{entropic}}$ to the HS model

$$\alpha_{\mathrm{entropic}}(\gamma) \propto \int_{\ell_{\min}}^{\ell_{\max}} \ell^3 P_{\mathrm{HS}}(\ell,\gamma)d\ell + \underbrace{\int_{\ell_{\min}}^{\ell_{\max}} \ell^3 f(\ell)d\ell}_{\alpha'_{\mathrm{entropic}} \propto}, \tag{D7}$$

this difference is moot when we take its γ deriviative as outlined above, to model $\tau(\gamma)$.

While the additional entropic term does not affect our model for the relaxation time, it does add some additional detail to the HS model. We obtain a "revised HS model" by recapitulating Helfrich and Servuss' derivation, this time using P_{Mell}. Their derivation assumes that the local inclination $\phi(\mathbf{r})$ is small ($\tan\phi \ll 1$) even at high wave number. At large ℓ, the amplitude of the undulations decays more slowly in P_{Mell} than in P_{HS} (see Fig. 2 in [26]), so we must check that the small ϕ assumption still holds.

For a given mode $u_\ell(\mathbf{r})$ with amplitude u_ℓ, we have $\tan(\phi_\ell) = |\nabla u_\ell(\mathbf{r})| \lesssim \ell u_\ell$. Since $P(\ell) \propto \langle u_\ell^2 \rangle$, we write

$$\frac{\langle \tan^2 \phi_{\ell,\text{Mell}} \rangle}{\langle \tan^2 \phi_{\ell,\text{HS}} \rangle} \lesssim \frac{P_{\text{Mell}}}{P_{\text{HS}}} \approx 1 + \left(\frac{12R}{hK_A}\right)\frac{\gamma + \kappa\ell^2}{1 + \frac{1}{2}hR\ell^2}. \tag{D8}$$

So if the small-ϕ approximation is valid for P_{HS} then it is valid for P_{Mell} as well, provided the term on the right hand side of Eq. (D8) is not too large. To obtain an upper bound on this term, we let the wave number go to infinity,

$$\lim_{\ell\to\infty}\left(\frac{12R}{hK_A}\right)\frac{\gamma + \kappa\ell^2}{1 + \frac{1}{2}hR\ell^2} = \frac{24\kappa}{h^2K_A} \Rightarrow \frac{P_{\text{Mell}}}{P_{\text{HS}}} \leqslant \left(1 + \frac{24\kappa}{h^2K_A}\right). \tag{D9}$$

Using $h_{\text{effective}} \approx 2$ nm, $R \lesssim 20\ \mu$m, $K_A \approx 0.1$ N/m, $\gamma \lesssim 1\ \mu$N/m, and $\kappa \approx 20 k_B T$, we have

$$\frac{P_{\text{Mell}}}{P_{\text{HS}}} \lesssim 6, \tag{D10}$$

with

$$\lim_{\ell\to 0}\frac{P_{\text{Mell}}}{P_{\text{HS}}} = \left(1 + \frac{12R\gamma}{hK_A}\right) \approx 2.2. \tag{D11}$$

The two spectra have the same order of magnitude, and therefore the weighting of modes used by Helfrich and Servuss [1] to integrate the area absorption over the spectrum of undulations remains valid:

$$(\Delta A)_\ell \propto -\ell^2 P(\ell,\gamma). \tag{D12}$$

Using P_{Mell} [Eq. (D5)], the entropic term in $\alpha(\gamma)$ becomes

$$\alpha_{\text{entropic}}(\gamma) = \frac{1}{4\pi}\int_{\ell_{\min}}^{\ell_{\max}} \ell^3 P_{\text{Mell}}(\ell,\gamma)d\ell \approx \frac{k_BT}{4\pi}\int_{\ell_{\min}}^{\ell_{\max}}\left[\frac{\ell}{\gamma + \kappa\ell^2} + \left(\frac{12R}{hK_A}\right)\frac{\ell}{1 + \frac{1}{2}hR\ell^2}\right]d\ell \tag{D13}$$

$$= \frac{k_BT}{4\pi}\left[\frac{1}{2\kappa}\ln\left(\frac{\gamma + \kappa\ell_{\min}^2}{\gamma + \kappa\ell_{\max}^2}\right) + \left(\frac{12}{h^2K_A}\right)\ln\left(\frac{1 + \frac{1}{2}hR\ell_{\min}^2}{1 + \frac{1}{2}hR\ell_{\max}^2}\right)\right]. \tag{D14}$$

Writing the cutoffs $\ell_{\min}^2 = \frac{\zeta}{A}, \ell_{\max}^2 = \frac{\zeta}{a}$, we arrive at a revised HS model:

$$\alpha(\gamma) \approx \underbrace{\frac{k_BT}{8\pi\kappa}\ln\left(\frac{\frac{\zeta}{A} + \frac{\gamma}{\kappa}}{\frac{\zeta}{a} + \frac{\gamma}{\kappa}}\right) + \frac{3k_BT}{\pi h^2K_A}\ln\left(\frac{1 + \frac{hR\zeta}{2A}}{1 + \frac{hR\zeta}{2a}}\right)}_{\text{entropic}} + \underbrace{\frac{\gamma}{K_A}}_{\text{direct}} \tag{D15}$$

[cf. Eq. (3.3)]. The middle term, which results from the high wave-number correction contained in P_{Mell}, shifts $\alpha(\gamma)$ by a constant but does not alter its tension dependence.

[1] W. Helfrich and R.-M. Servuss, Undulations, steric interaction and cohesion of fluid membranes, Nuovo Cimento D **3**, 137 (1984).

[2] K. Haase and A. E. Pelling, Resiliency of the plasma membrane and actin cortex to large-scale deformation, Cytoskeleton **70**, 494 (2013).

[3] E. Schäfer, T.-T. Kliesch, and A. Janshoff, Mechanical properties of giant liposomes compressed between two parallel plates: Impact of artificial actin shells, Langmuir **29**, 10463 (2013).

[4] E. Schäfer, M. Vache, T.-T. Kliesch, and A. Janshoff, Mechanical response of adherent giant liposomes to indentation with a conical AFM-tip, Soft Matter **11**, 4487 (2015).

[5] L. Guolla, M. Bertrand, K. Haase, and A. E. Pelling, Force transduction and strain dynamics in actin stress fibres in response to nanonewton forces, J. Cell Sci. **125**, 603 (2012).

[6] Z. Al-Rekabi and A. E. Pelling, Cross talk between matrix elasticity and mechanical force regulates myoblast traction dynamics, Phys. Biol. **10**, 066003 (2013).

[7] A. L. Hemsley, D. Hernandez, C. Mason, A. Pelling, and F. Veraitch, Precisely delivered nanomechanical forces induce blebbing in undifferentiated mouse embryonic stem cells, Cell Health Cytoskeleton **3**, 23 (2011).

[8] Y. R. Silberberg, A. E. Pelling, G. E. Yakubov, W. R. Crum, D. J. Hawkes, and M. A. Horton, Mitochondrial displacements in response to nanomechanical forces, J. Mol. Recognit. **21**, 30 (2008).

[9] M. Bertrand and B. Joós, Extrusion of small vesicles through nanochannels: A model for experiments and molecular dynamics simulations, Phys. Rev. E **85**, 051910 (2012).

[10] J. A. Anderson, C. D. Lorenz, and A. Travesset, General purpose molecular dynamics simulations fully implemented on graphics processing units, J. Comput. Phys. **227**, 5342 (2008).

[11] HOOMD-blue web page, 2015, http://codeblue.umich.edu/hoomd-blue/.
[12] C. L. Phillips, J. A. Anderson, and S. C. Glotzer, Pseudo-random number generation for Brownian dynamics and dissipative particle dynamics simulations on GPU devices, J. Comput. Phys. **230**, 7191 (2011).
[13] A. Arnold, O. Lenz, S. Kesselheim, R. Weeber, F. Fahrenberger, D. Roehm, P. Košovan, and C. Holm, ESPResSo 3.1: Molecular dynamics software for coarse-grained models, in *Meshfree Methods for Partial Differential Equations VI*, edited by M. Griebel and M. A. Schweitzer, Lecture Notes in Computational Science and Engineering No. 89 (Springer, Berlin, 2013), pp. 1–23.
[14] ESPResSo homepage, 2015, http://espressomd.org.
[15] J. Hunter, Matplotlib: A 2d graphics environment, Comput. Sci. Eng. **9**, 90 (2007).
[16] matplotlib homepage, 2015, http://matplotlib.org.
[17] N. Michaud-Agrawal, E. J. Denning, T. B. Woolf, and O. Beckstein, MDAnalysis: A toolkit for the analysis of molecular dynamics simulations, J. Comput. Chem. **32**, 2319 (2011).
[18] MDAnalysis homepage, 2015, http://www.mdanalysis.org.
[19] S. van der Walt, S. Colbert, and G. Varoquaux, The NumPy Array: A structure for efficient numerical computation, Comput. Sci. Eng. **13**, 22 (2011).
[20] NumPy and SciPy documentation, 2015, http://docs.scipy.org/doc/.
[21] R. Goetz and R. Lipowsky, Computer simulations of bilayer membranes: Self-assembly and interfacial tension, J. Chem. Phys. **108**, 7397 (1998).
[22] M. Bertrand, *Deformed Soft Matter under Constraints*, Ph.D. thesis, University of Ottawa, 2012.
[23] N. Amenta, M. Bern, and M. Kamvysselis, A new Voronoi-based surface reconstruction algorithm, in *Proceedings of the 25th Annual Conference on Computer Graphics and Interactive Techniques, SIGGRAPH '98* (ACM, New York, 1998), pp. 415–421.
[24] E. Evans and W. Rawicz, Entropy-Driven Tension and Bending Elasticity in Condensed-Fluid Membranes, Phys. Rev. Lett. **64**, 2094 (1990).
[25] R. Dimova, N. Bezlyepkina, M. D. Jordö, R. L. Knorr, K. A. Riske, M. Staykova, P. M. Vlahovska, T. Yamamoto, P. Yang, and R. Lipowsky, Vesicles in electric fields: Some novel aspects of membrane behavior, Soft Matter **5**, 3201 (2009).
[26] M. Mell, L. H. Moleiro, Y. Hertle, I. López-Montero, F. J. Cao, P. Fouquet, T. Hellweg, and F. Monroy, Fluctuation dynamics of bilayer vesicles with intermonolayer sliding: Experiment and theory, Chem. Phys. Lipids **185**, 61 (2015).
[27] R. Dimova, K. A. Riske, S. Aranda, N. Bezlyepkina, R. L. Knorr, and R. Lipowsky, Giant vesicles in electric fields, Soft Matter **3**, 817 (2007).
[28] K. A. Riske and R. Dimova, Electro-deformation and poration of giant vesicles viewed with high temporal resolution, Biophys. J. **88**, 1143 (2005).
[29] W. K. den Otter and S. A. Shkulipa, Intermonolayer friction and surface shear viscosity of lipid bilayer membranes, Biophys. J. **93**, 423 (2007).
[30] S. A. Shkulipa, W. K. d. Otter, and W. J. Briels, Simulations of the dynamics of thermal undulations in lipid bilayers in the tensionless state and under stress, J. Chem. Phys. **125**, 234905 (2006).
[31] W. K. den Otter, Area compressibility and buckling of amphiphilic bilayers in molecular dynamics simulations, J. Chem. Phys. **123**, 214906 (2005).
[32] R. Goetz, G. Gompper, and R. Lipowsky, Mobility and Elasticity of Self-Assembled Membranes, Phys. Rev. Lett. **82**, 221 (1999).
[33] A. Grafmüller, J. Shillcock, and R. Lipowsky, The fusion of membranes and vesicles: Pathway and energy barriers from dissipative particle dynamics, Biophys. J. **96**, 2658 (2009).
[34] C. Das, K. H. Sheikh, P. D. Olmsted, and S. D. Connell, Nanoscale mechanical probing of supported lipid bilayers with atomic force microscopy, Phys. Rev. E **82**, 041920 (2010).
[35] N. Fa, L. Lins, P. J. Courtoy, Y. Dufrêne, P. Van Der Smissen, R. Brasseur, D. Tyteca, and M. P. Mingeot-Leclercq, Decrease of elastic moduli of DOPC bilayers induced by a macrolide antibiotic, azithromycin, Biochim. Biophys. Acta, Biomembr. **1768**, 1830 (2007).
[36] S. Moreno-Flores and R. Benítez, Comment on "Mechanical properties of giant liposomes compressed between two parallel plates: Impact of artificial actin shells", Langmuir **30**, 7928 (2014).
[37] K. Fricke and E. Sackmann, Variation of frequency spectrum of the erythrocyte flickering caused by aging, osmolarity, temperature and pathological changes, Biochim. Biophys. Acta, Mol. Cell Res. **803**, 145 (1984).
[38] H. Karcher, J. Lammerding, H. Huang, R. T. Lee, R. D. Kamm, and M. R. Kaazempur-Mofrad, A three-dimensional viscoelastic model for cell deformation with experimental verification, Biophys. J. **85**, 3336 (2003).
[39] N. Desprat, A. Richert, J. Simeon, and A. Asnacios, Creep function of a single living cell, Biophys. J. **88**, 2224 (2005).
[40] B. A. Smith, B. Tolloczko, J. G. Martin, and P. Grütter, Probing the viscoelastic behavior of cultured airway smooth muscle cells with atomic force microscopy: Stiffening induced by contractile agonist, Biophys. J. **88**, 2994 (2005).
[41] O. Thoumine and A. Ott, Time scale dependent viscoelastic and contractile regimes in fibroblasts probed by microplate manipulation, J. Cell Sci. **110**, 2109 (1997).
[42] T. Yeung, P. C. Georges, L. A. Flanagan, B. Marg, M. Ortiz, M. Funaki, N. Zahir, W. Ming, V. Weaver, and P. A. Janmey, Effects of substrate stiffness on cell morphology, cytoskeletal structure, and adhesion, Cell Motil. Cytoskeleton **60**, 24 (2005).
[43] R. J. Pelham and Y.-l. Wang, Cell locomotion and focal adhesions are regulated by substrate flexibility, Proc. Natl. Acad. Sci. USA **94**, 13661 (1997).
[44] A. Alessandrini and P. Facci, AFM: A versatile tool in biophysics, Meas. Sci. Technol. **16**, R65 (2005).
[45] M. Yoneda, Tension at the surface of sea-urchin egg: A critical examination of Cole's experiment, J. Exp. Biol. **41**, 893 (1964).
[46] E. A. Evans and R. Skalak, *Mechanics and Thermodynamics of Biomembranes* (CRC Press, Boca Raton, FL, 1980).